Proceedings of Global Power and Propulsion Society
ISSN-Nr: 2504-4400
GPPS Chania24
September 4-6, 2024
www.gpps.global

GPPS-TC-2024-0054

A HARMONIC BALANCE SOLVER FOR THE AEROELASTIC ANALYSIS OF TURBOMACHINERY COMPONENTS ON UNSTRUCTURED GRIDS

Hans-Peter Kersken
German Aerospace Center (DLR)
hans-peter.kersken@dlr.de
Cologne, Germany

Pierre Sivel
German Aerospace Center (DLR)
pierre.sivel@dlr.de
Cologne, Germany

Michael Müller
German Aerospace Center (DLR)
mi.mueller@dlr.de
Cologne, Germany

Christian Frey
German Aerospace Center (DLR)
christian.frey@dlr.de
Cologne, Germany

ABSTRACT

The harmonic balance method has proven to be an efficient tool for the study of aeroelastic phenomena associated with blades in turbomachinery components. In the turbomachinery industry it is used, for example, to predict the flutter susceptibility of blades using structured meshes. For the analysis of more complex geometries, like cavities or labyrinth seals, unstructured grids are easier to create than structured ones to accurately model geometric details of these components. With this application in mind, specifically the flutter analysis of labyrinth seals, an existing harmonic balance solver for the unsteady Reynolds averaged Navier-Stokes equations on structured grids has been extended to work efficiently on unstructured grids. Although the harmonic balance algorithm itself is agnostic to the spatial discretization method, as it is only related to the discretization in time, some adaptations are necessary for an efficient implementation. To verify the extensions for unstructured grids, the harmonic balance solver is applied to the flutter analysis of a NACA airfoil exhibiting an oscillating shock-induced separation region. To demonstrate the ability to handle unstructured mixed-element grids, a flutter analysis of a generic labyrinth seal test case on an unstructured grid is performed.

INTRODUCTION

Aeroelastic analysis using high fidelity CFD methods has become a standard tool in the design of compressor and turbine components like blades and, more recently, of small scale parts like cooling channels or labyrinth seals. These geometrical details can be sources of disturbances which may excite blade vibrations or their structural stability may be a matter of concern by itself. To accurately model the geometry of the small scale geometrical features, the construction of structured meshes is known to be tedious due to the large number of details to be captured. The use of unstructured meshes has some advantages for these small scale parts while for the main flow path structured meshes are the method of choice having performance advantages. A hybrid meshing approach could be used when studying the aerodynamic and aeroelastic behaviour of a turbomachinery component. To investigate the complex phenomena, efficient numerical methods capable of accurately capturing the underlying unsteady interaction between the structure and aerodynamic flow field are required. The physical phenomenon of flutter is controlled by the frequencies of the structural modes of the component. Perturbations with these frequencies often dominate the unsteadiness in the aerodynamic flow field. In these cases results with sufficient accuracy can be obtained efficiently by restricting the simulation to these frequencies. Therefore, the susceptibility of a structural mode with respect to flutter is often studied by means of simulation methods formulated in the frequency-domain.

The paper is organized as follows: First a concise summary of the harmonic balance (HB) algorithm is given. Then the modifications to the implementation are explained which are necessary when extending the existing HB implementation to unstructured grids. Finally, two cases employing unstructured grids for aeroelastic analysis are presented. First the flutter analysis of a NACA3506 profile is performed where the flow exhibits a strong shock boundary layer interaction. This case is described in detail in (Müller et al., 2022). Second a generic labyrinth seal configuration introduced in (Corral et al., 2021) is studied. The results are compared to those obtained on a structured grid.

NUMERICAL METHOD

The HB method used in this work is part of the CFD code TRACE (Becker et al., 2010) developed at DLR's Institute of Propulsion Technology in close cooperation with MTU Aero Engines to study turbomachinery flows. It solves the steady and unsteady compressible Reynolds-averaged Navier-Stokes (RANS) equations on hybrid grids, comprising both structured and unstructured grid blocks in the relative frame of reference via a finite-volume discretization using a multi-block approach. For completeness, we will first summarize the HB algorithm as it is implemented in TRACE. For a detailed description see (Frey et al., 2014). Then the spatial discretization is described and the necessary modifications to the algorithm are explained when it is applied on unstructured grids. For details of the discretization on structured grid refer to (Franke et al., 2010) and for a detailed description of the unstructured discretization see (Becker and Ashcroft, 2014).

Harmonic Balance Method

For the present work it is sufficient to note that after discretizing the spatial operators in the RANS equations the following system of ordinary differential equations is obtained irrespective of the grid type.

$$\frac{d\mathbf{q}}{dt} + \mathbf{R}(\mathbf{q}(t)) = 0 \tag{1}$$

where $\mathbf{q}$ is the vector of conservative variables, $\mathbf{R}$ is the discretized RANS residual vector and t denotes the physical time. Time-periodic solutions of Eqn. (1) can be described by a limited number of solution harmonics, i.e.,

$$\mathbf{q}(x,t) = \mathrm{Re}\left[\sum_{k=0}^{K} \widehat{\mathbf{q}}_k(x) e^{ik\omega t}\right] \tag{2}$$

where $\widehat{\mathbf{q}}_k$ are the complex valued solution harmonics and ω is the fundamental angular frequency. In such cases it is computationally attractive to formulate the unsteady problem, Eqn. (1), in the frequency domain. By inserting Eqn. (2) into Eqn. (1) a system of equations of the form

$$\mathbf{i}k\omega\widehat{\mathbf{q}}_k + \widehat{\mathbf{R}(\mathbf{q})}_k = 0 \tag{3}$$

for only a finite number of harmonics, $k = 0,\ldots,K$, is obtained. To compute the harmonics $\widehat{\mathbf{R}(\mathbf{q})}_k$ of the RANS residual vector $\mathbf{R}$ the solution field vector is first reconstructed at N sampling points from the harmonics of the conservative variables $\widehat{\mathbf{q}}_k$ using the inverse discrete Fourier transform (DFT). With the reconstructed solution vectors, the RANS residual vectors $\mathbf{R}$ are then computed at these sampling points. Taking the DFT of $\mathbf{R}$ gives the Fourier coefficients of the residual $\widehat{\mathbf{R}(\mathbf{q})}_k$. That is, $\widehat{\mathbf{R}(\mathbf{q})}_k$ is computed as $\mathscr{F}(\mathbf{R}(\mathscr{F}^{-1}\widehat{\mathbf{q}}))|_k$, where $\mathscr{F}$ denotes the DFT and $\mathscr{F}^{-1}$ its inverse. Hence, we solve

$$\mathbf{i}k\omega\widehat{\mathbf{q}}_k + \mathscr{F}(\mathbf{R}(\mathscr{F}^{-1}\widehat{\mathbf{q}}))|_k = 0 \tag{4}$$

in the frequency domain to obtain the complex valued harmonics of the conservative variables $\widehat{\mathbf{q}}_k$.

Note that, since the RANS residual $\mathbf{R}$ is evaluated in the time-domain the numerical flux and discretization scheme of the underlying nonlinear solver can be used. As a hybrid time- and frequency-domain method the approach has the advantage, over methods formulated purely in the time- or frequency-domain, of being able to employ not only the possibly highly nonlinear time-domain flux functions (and their stabilizing numerical limiters) but also highly accurate nonreflecting boundary conditions formulated in the frequency domain (Giles, 1990). Particularly in the context of aeroelasticity analysis and aeroacoustics boundary conditions are of utmost importance. The implementation in TRACE of these boundary conditions is described in (Kersken et al., 2014). For aeroelastic analysis the approach described above has to be modified to deal with time-dependent meshes as described in (Ashcroft et al., 2014).

Harmonic Balance Method For Unstructured Grids

So far no reference to a specific spatial discretization method has been made because only the temporal discretization has been considered which can be applied unaltered to structured and unstructured meshes. To understand the differences between the HB implementation for structured and unstructured grids we have to look into the spatial discretization of the numerical fluxes in detail. In a cell centered finite volume solver, the residual at a cell is the sum of convective and viscous fluxes at its faces, $\mathbf{F}_{s,\mathrm{conv}}$ and $\mathbf{F}_{s,\mathrm{visc}}$, respectively, apart from source terms, which depends on the state of the cell itself only:

$$\mathbf{F}_s(\mathbf{q}) = \mathbf{F}_{s,\mathrm{conv}}(\mathbf{q}_\mathrm{L}, \mathbf{q}_\mathrm{R}) + \mathbf{F}_{s,\mathrm{visc}}((\nabla\mathbf{q})_s). \tag{5}$$

The convective fluxes $\mathbf{F}_{s,\mathrm{conv}}$ are computed using left and right states, ($\mathbf{q}_\mathrm{L}$ and $\mathbf{q}_\mathrm{R}$), at face s straddled by cells i and i' which are computed with second order accurate extrapolation schemes, i.e., on structured grids,

$$\mathbf{q}_\mathrm{L} = \mathbf{q}_i + \frac{1}{2}(\widetilde{\Delta}\mathbf{q})_\mathrm{L}, \quad \mathbf{q}_\mathrm{R} = \mathbf{q}_{i'} - \frac{1}{2}(\widetilde{\Delta}\mathbf{q})_\mathrm{R}, \tag{6}$$

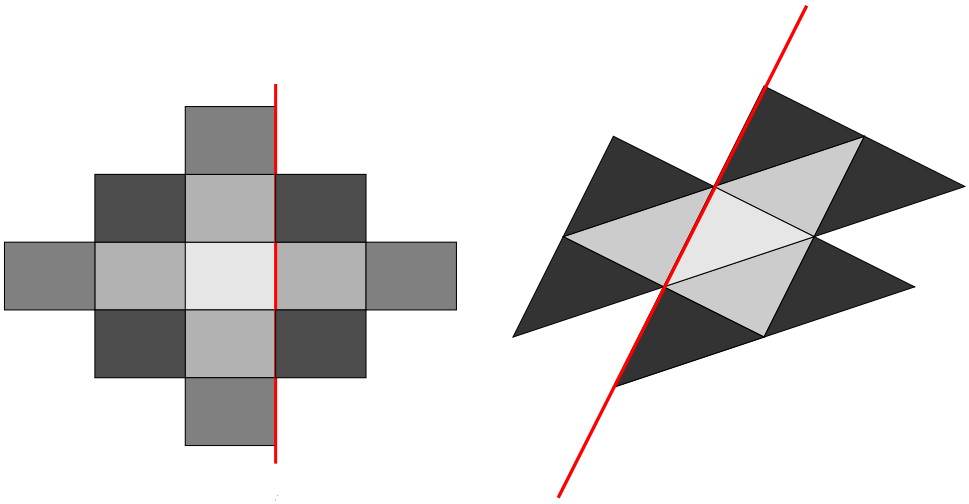

Figure 1 Stencil for the second order RANS residual computation on structured and unstructured meshes.

whereas, on unstructured grids,

$$\mathbf{q}_{\mathrm{L}} = \mathbf{q}_i + (\widetilde{\nabla}\mathbf{q})_{\mathrm{L}} \cdot (x_s - x_i), \quad \mathbf{q}_{\mathrm{R}} = \mathbf{q}_{i'} + (\widetilde{\nabla}\mathbf{q})_{\mathrm{R}} \cdot (x_s - x_{i'}) \tag{7}$$

is used. By $(\widetilde{\Delta}\mathbf{q})_{\mathrm{L/R}}$ and $(\widetilde{\nabla}\mathbf{q})_{\mathrm{L/R}}$ we denote the limited slopes and gradients at cell centers, respectively, see (Blazek, 2001) and (Becker and Ashcroft, 2014) for details. The cell gradients are computed using the Least-Squares-Fully-Augmented (LSFA) approach. Computation of viscous fluxes require gradient at cell faces. These are computed following (Thomas et al., 2011) by averaging the gradients at the cells straddling the face and adding a damping term depending on the tangential component of the average.

At block boundaries in a multi-block configuration additional implementations have to be considered for both unstructured and structured grids. Fig. 1 depicts the situation for a two-dimensional grid with the focus on a single stencil where the red line marks the block boundaries. Neighbouring cells may reside on different blocks, however, their values are needed to maintain second order spatial accuracy across block boundaries. For structured grid this is solved by exchanging a two cell wide ghost cell layer surrounding each block which is filled with the respective values from neighbouring blocks. With these values the second order extrapolation can be performed locally at block boundaries. In Fig. 1 these are the cells to the right of the red line for the structured stencil. This procedure for structured grids does not carry over to unstructured grids because in TRACE we keep only one layer of ghost cells on unstructured grids which is constructed from cells having a common face with the local cell. The gradient in these cells however can not be computed locally because information on the neighbourhood of the ghost cell, the black triangles to the left of the red line in the right picture in Fig. 1, is incomplete. Therefore, in the steady and unsteady solver in the time domain a two-step process is used here. First the states at the ghost cells are exchanged which allows the gradients at the cells adjacent to the boundary to be computed locally. Then the gradients are exchanged which, in turn, allows to compute the state at the ghost cell side of the face, required for second order spatial accuracy, and the gradients at the face, necessary for the computation of viscous fluxes.

In the HB context we have to compute the nonlinear residual for every sampling point t_p used to compute the harmonics of the residual $\widehat{\mathbf{R}(\mathbf{q})}_k = \mathscr{F}(\mathbf{R}(\mathscr{F}^{-1}\widehat{\mathbf{q}}))|_k$ from the reconstructed states $\mathbf{q}(t_p) = \mathscr{F}^{-1}\widehat{\mathbf{q}}$ and its gradients $\nabla\mathbf{q}(t_p)$ at the cell itself and its neighbours. If we follow the two-step process described above this procedure has to be repeated for every sampling point, i.e., two communications steps are initiated for every sampling point each blocking the computation. It would be preferable to cluster or even avoid these communication steps. Taking the gradients at ghost cells not into account would reduce the spatial discretization order from second to first order at block boundaries. However, observe that the inverse DFT and the computation of the gradients are linear operations which commute, $\nabla\mathbf{q} = \nabla(\mathscr{F}^{-1}\widehat{\mathbf{q}}) = \mathscr{F}^{-1}(\nabla\widehat{\mathbf{q}})$. Therefore, instead of computing the gradients of the states at ghost cells by the two-step procedure at every sampling point they can be reconstructed from the gradients of the harmonics. This is achieved by first exchanging the harmonics $\widehat{\mathbf{q}}_k$ and computing their gradients locally at cells which are ghost cells at neighbouring blocks and pass them to the neighboring block. This happens once per iteration step before computing the Fourier transform of the residual. Now the gradients at ghost cells can be reconstructed from their harmonics locally for computing the nonlinear residual at every sampling point without further communication steps.

In addition to the algorithm described in (Kersken et al., 2016) for the Euler equations the HB algorithm for unstructured has been extended to solve for the higher harmonics of turbulence and transition model variables as well. It turned out that if viscous fluxes are taken into account the accuracy of the implemented algorithm for computing the mesh deformation,

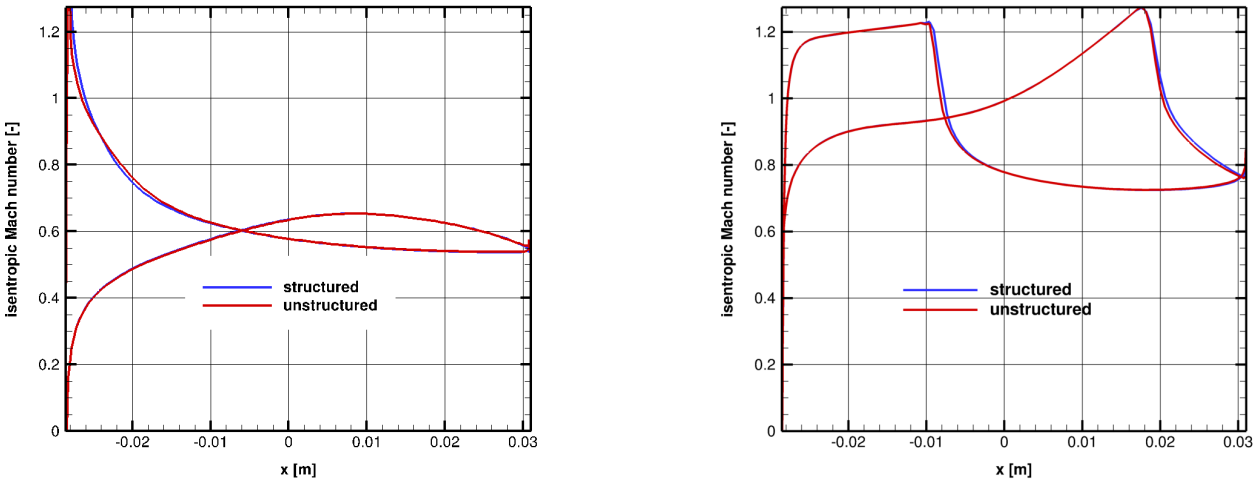

(a) Subsonic case. **(b) Transonic case.**

Figure 2 NACA3506: Isentropic Mach number at midspan.

necessary for flutter analysis, was insufficient at block boundaries. This inaccuracy caused severe convergence problems especially in the boundary layer in presence of stretched cells. The accuracy of the algorithm could be improved by an additional smoothing of the perturbation of the grid coordinates at block boundaries.

APPLICATIONS

The method described in the previous section has been applied to two configurations and simulation results are compared to those obtained on structured grids.

NACA3605 Profile

This test case is described in detail in (Müller et al., 2022) and used there, employing a structured grid, to demonstrate the advantages of the k-log(ω) formulation of the Wilcox k-ω turbulence model (Wilcox, 2006) over the original one in the context of flutter analysis in computational challenging configurations due to strong unsteady shock boundary layer interactions in terms of stability and convergence rate. For the simulations reported here, the baseline grid, comprising about 62,000 hexahedral cells with three cells in radial direction, was converted to an unstructured topology, see Fig 4, and the standard k-ω turbulence model was used. A subsonic and a transonic operation point, the latter displays shocks on suction and pressure side, have been studied. At the outlet the static pressure was set to 220 kPa for the subsonic case and 205.5 kPa for the transonic case. For both cases the inlet boundary conditions for the flow have been set to a stagnation pressure and a stagnation temperature of 293 kPa and 293 K, respectively, and an inflow angle of 45°. For the turbulence model a turbulence intensity of 2% and turbulence length scale of 4.5×10^{-5}m were specified at the inlet. A translational movement normal to the chord, representing a bending mode, with a frequency of 227 Hz and an amplitude of 1.25 % of the chord length was added for the flutter simulation. With this movement, the flow displays flow phenomena similar to those examined by Duquesne (Duquesne et al., 2019) and Heners et al. (Heners et al., 2022). In this case, the shock at the pressure side interacts strongly with the boundary layer, making the correct time dependent treatment of turbulence important. For the steady solution the isentropic Mach number around the blade is shown in Fig. 2. Figure 2b clearly display the shocks on pressure and suction side in the transonic case while there is none shown for the subsonic case in Fig. 2a.

A structural mode modelled by a translational movement of the blade normal to the chord, representing a bending mode, with a frequency of 227 Hz and an amplitude of 1.25 % of the chord length has been prescribed. The damping curves were computed by varying the inter blade phase angle (IBPA) of the mode. The analysis has been performed with three higher harmonics for both the flow variables and the variables of the turbulence model. Three higher harmonics have been found to be necessary for obtaining harmonic convergence in the transonic case in (Müller et al., 2022).

The damping curves obtained on both the structured and the unstructured grids are shown in Fig. 3 which displays an almost perfect agreement for the subsonic case and an overall good agreement for the transonic case. The deviation from sine shape for the subsonic case and the pronounced peak in the damping curve for the transonic case can be explained by the presence of acoustic resonances. From estimates of the cut-off ratio for acoustic modes, using average flow velocities in circumferential and axial direction, acoustic resonances are predicted at an IBPA of about -25°and +10°for the subsonic case and about -35°and +6°for the transonic case distorting the damping curve for IBPAs in their vicinity. The main cause for the difference between the simulations on the structured and unstructured grid observed for the transonic case is the slightly different shock position predicted which is already visible for the steady simulation, see Fig. 2b. As an example

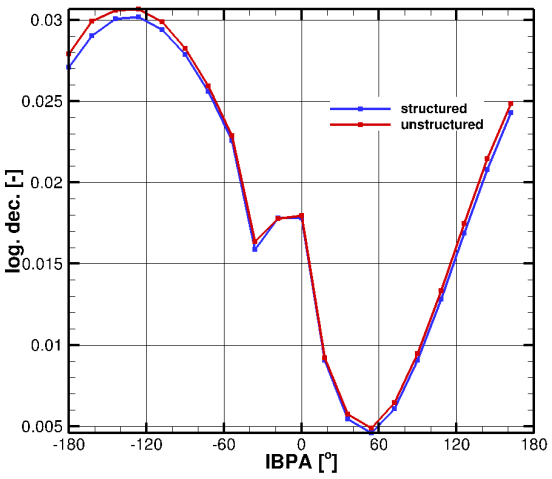

(a) Subsonic case.

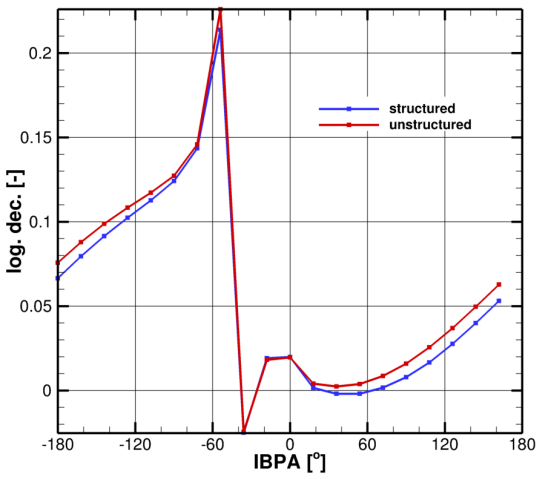

(b) Transonic case.

Figure 3 NACA3605: Damping curves.

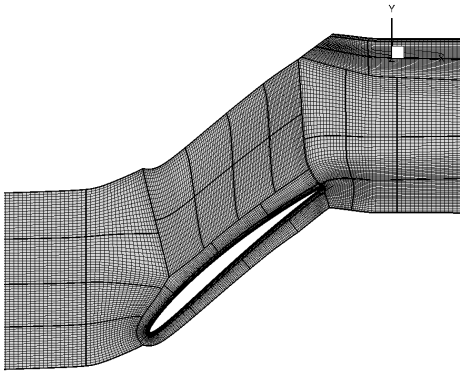

Figure 4 NACA3506: Mesh and block topology at midspan.

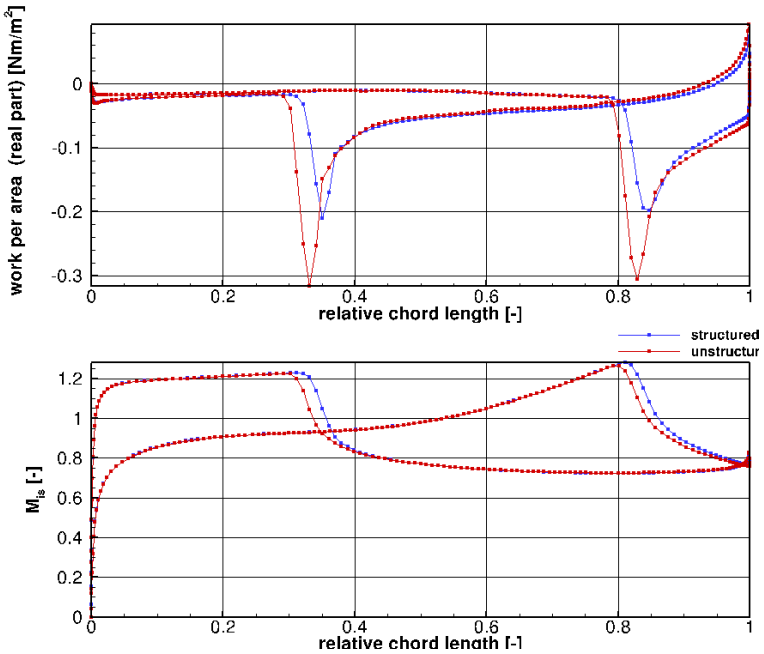

Figure 5 Real part of the work per area of the first harmonic (top) and the isentropic Mach number of the time averaged solution (bottom) for IBPA=180°.

Fig. 5 depicts the isentropic Mach number and the real part of the work per cycle and area along the blade showing that its peaks are aligned with the shock positions on both grids.

Generic Labyrinth Seal

The second test case is a configuration proposed in (Greco and Corral, 2021) to validate an analytically derived formula for the aeroelastic work exerted on a generic labyrinth seal. A two fin labyrinth seal is straddled by two large relaxation chambers to avoid resonance effects and ensure uniform pressure at the entry and exit of the seal gaps. Figure 6 shows a meridional cut of its rotational symmetric geometry including all relevant geometrical quantities defining the computational domain. In (Corral et al., 2021; Greco and Corral, 2021) the cavity radius, the cavity height, the seal clearance and the inter-fin distance were defined. Missing geometrical parameters were extracted from the figures in the cited publications and may differ slightly from the original test case. The structured mesh is similar to the one used in (Sivel et al., 2024). It comprises about 350000 hexahedral cells with 10 cells in circumferential direction and a pitch segment of 10°. A completely unstructured mesh has been created using CENTAUR (*Centaur Software*, 2024). In contrast to the structured set-up the

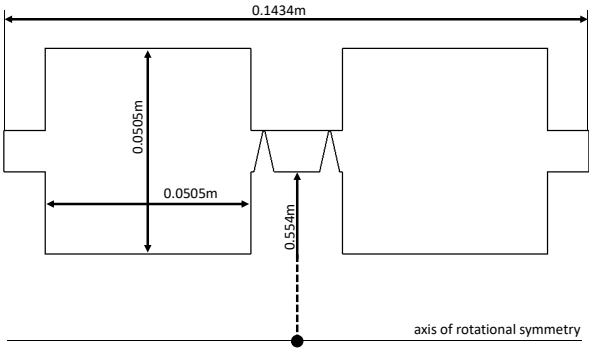

(a) Outline of the computaitonal domain.

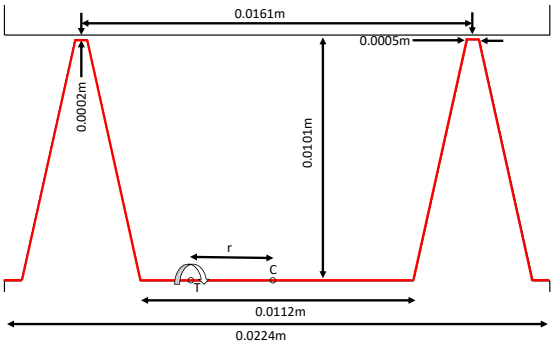

(b) Geometric detail of the seal. Marked in red is the surface of the seal where the torsion mode is applied. The center of the seal bottom and the torsion center are inidcated by C and T, respectively.

Figure 6 Computational domain and dimensions of the generic labyrinth seal.

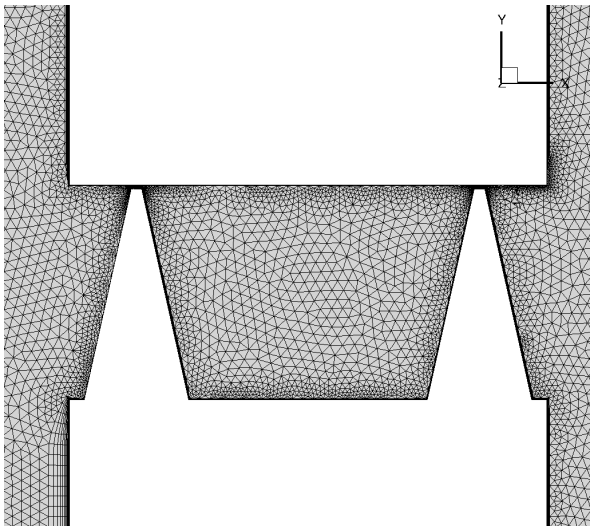

(a) Close-up of the unstrucutred mesh at the seal cavity.

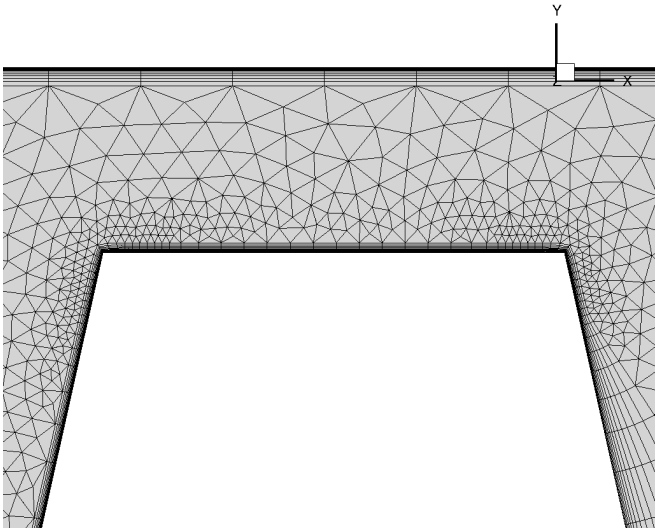

(b) Close-up of the mesh in the gap of the upstream seal fin.

Figure 7 Close-up of the unstrucutred mesh of the generic labyrinth seal.

circumferential extension was chosen to be 0.1°only to reduce the cell count for a completely unstructured mesh. The unstructured mesh comprises about 1.1×10^6 cells; prisms to resolve the boundary layer, hexahedral cells in the inlet and outlet ducts, tetrahedral cells in the interior and pyramids to connect tetrahedral cells to hexahedral cells. Figure 7 shows details of the unstructured mesh in the seal cavity and the seal gap. $y^+ < 1$ has been ensured on both grids for the steady solution at all solid boundaries using low-Reynolds no-slip boundary condition. The turbulence is modelled by the Wilcox k-ω turbulence model (Wilcox, 2006) in combination with the Kato Launder stagnation point anomaly fix (Kato and Launder, 1993).

At inlet the stagnation temperature, the stagnation pressure, and the inflow direction (parallel to the x-axes) and at the outlet the static pressure are prescribed. The pressure ratio is $\pi_T = p_{t,\,\text{inlet}}/p_{\text{outlet}} = 1.5$ and the Reynolds number based on the fin clearance and the inlet velocity is $Re \approx 25{,}000$. The flow is subsonic in the whole domain with a maximal Mach number of about 0.65 at the clearance of the fins. For flutter analysis, torsion modes are prescribed on the seal surface (depicted in red in Fig. 6b). The torsion center is positioned at the same radius as the bottom of the inter-fin cavity, at different axial distances from the center of the cavity, defined by the torsion radius r (see Fig. 6b) and the frequency is taken to be 423.6 Hz. The frequency and torsion radii are the same as used in (Sivel et al., 2024). The prescribed torsion amplitude for each torsion radius is adapted to ensure a maximum displacement at the fin tip of 0.1% of the fin clearance. All HB computations are initialized with a steady-state solution and the first harmonic of the flow and turbulent quantities is included in the computations. Figure 8 shows the Mach number distribution and streamlines of the time averaged flow field in the cavity for a simulation with with $r = 0.0087m$ for ND=6 at a circumferential position of 0°.

Figure 9 shows a comparison of the real part of the aerodynamic work per cycle integrated over the seal surface for

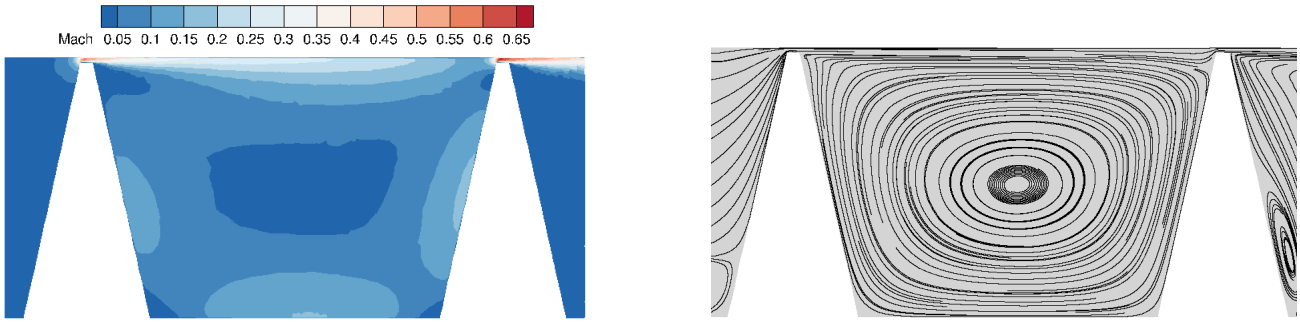

(a) Mach number (b) Streamlines

Figure 8 The time averaged flow field inside the cavity for a torsion radius r=0.0087m and ND=6.

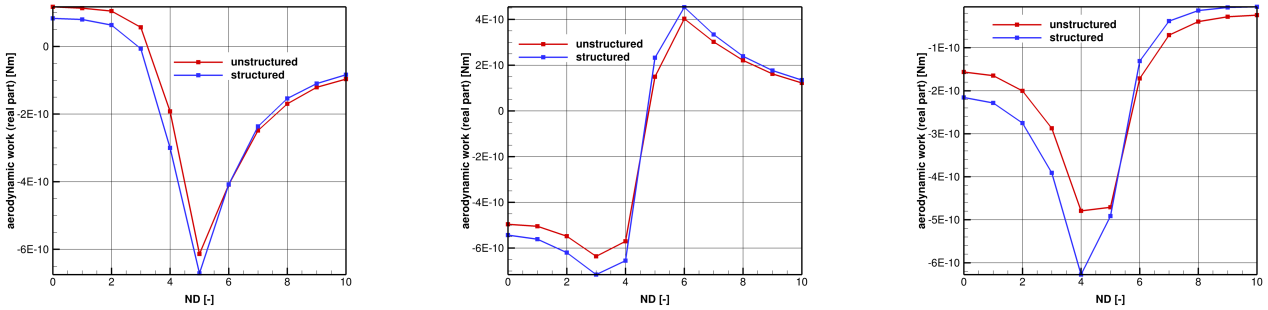

(a) r=-0.069m (b) r=0.0087m (c) r=0.122m

Figure 9 Aerodynamic work per cycle for different posisitons of the torsion center.

different positions of the torsion axis, i.e, torsion radii. The results of the computations on the structured grid are scaled by 0.01 to accommodate to the larger circumferential extension of the structured mesh. In the cases where the center is close to the rotation axis the agreement is excellent. For the case with torsion radius 0.122 m the difference between the results on the structured and unstructured grid is larger especially for the peak value. For all three cases the nodal diameter of the peak value and the region of stability is predicted in accordance with the structured results. The cause for the larger differences in the case with torsion radius 0.122 m is subject to further analysis.

SUMMARY AND OUTLOOK

In this paper we described a Harmonic Balance solver for unstructured multi-block grids for the URANS equations. An existing HB solver for the Euler equations has been extended to solve the URANS equations including the turbulence model. The solver has been applied to two test configurations: a single blade with subsonic and transonic flow conditions and a generic labyrinth seal configuration. Results on structured and unstructured grids have been compared and found in good agreement in general. The results of the flutter analysis for the blade at the subsonic operation point were in very good agreement while for the transonic operation point some differences have been observed which could be related to slightly different shock positions predicted by the structured and unstructured solver. The results for the aeroelastic analysis of a generic labyrinth seal, obtained on a completely unstructured grid, have been found to be in good agreement with the results on a structured grid.

After this verification of the Harmonic Balance solver for unstructured grids it is planned to employ it for the aeroelastic stability analysis of labyrinth seals in a multi-stage configurations.

NOMENCLATURE

ND	nodal diameter
Re	Reynolds number
π_T	pressure ratio
$\mathbf{R}$	nonlinear time domain residual
$\mathbf{q}$	state vector
$\mathbf{F}$	flux vector
V	cell volume
$\mathscr{F}$	discrete Fourier transform
$\widehat{a}$	Fourier coefficient of quantity a
Re	real part of a complex number
ω	angular frequency
$\mathbf{i}$	imaginary unit
t	time
τ	pseudo-time
p	static pressure
p_t	total pressure
y^+	non-dimensional normal wall distance

REFERENCES

References

Ashcroft, G., Frey, C. and Kersken, H.-P. (2014), On the development of a harmonic balance method for aeroelastic analysis, *in* '6th European Conference on Computational Fluid Dynamics (ECFD VI)', pp. 5885–5897.

Becker, K. C. and Ashcroft, G. (2014), A comparative study of gradient reconstruction methods for unstructured meshes with application to turbomachinery flows, *in* 'AIAA SciTech', American Institute of Aeronautics and Astronautics.
URL: *http://dx.doi.org/10.2514/6.2014-0069*

Becker, K., Heitkamp, K. and Kügeler, E. (2010), Recent progress in a hybrid-grid CFD solver for turbomachinery flows, *in* 'Proceedings Fifth European Conference on Computational Fluid Dynamics ECCOMAS CFD 2010', Lisbon, Portugal.
URL: *http://congress2.cimne.com/eccomas/proceedings/cfd2010/papers/01609.pdf*

Blazek, J. (2001), *Computational fluid dynamics: principles and applications*, Elsevier Science.

Centaur Software (2024), https://www.centaursoft.com.

Corral, R., Greco, M. and Vega, A. (2021), 'Higher order conceptual model for labyrinth seal flutter', *Journal of Turbomachinery* **143**(7).

Duquesne, P., Rendu, Q., Aubert, S. and Ferrand, P. (2019), 'Choke flutter instability sources tracking with linearized calculations', *International Journal of Numerical Methods for Heat & Fluid Flow* .

Franke, M., Röber, T., Kügeler, E. and Ashcroft, G. (2010), Turbulence treatment in steady and unsteady turbomachinery flows, *in* 'Proceedings Fifth European Conference on Computational Fluid Dynamics ECCOMAS CFD 2010', Lisbon, Portugal.
URL: *http://congress2.cimne.com/eccomas/proceedings/cfd2010/papers/01628.pdf*

Frey, C., Ashcroft, G., Kersken, H.-P. and Voigt, C. (2014), A harmonic balance technique for multistage turbomachinery applications, *in* 'ASME Turbo Expo 2014: Turbine Technical Conference and Exposition', p. V02BT39A005.
URL: *http://dx.doi.org/10.1115/GT2014-25230*

Giles, M. B. (1990), 'Nonreflecting boundary conditions for Euler calculations', *AIAA J.* **28**(12), 2050–2058.

Greco, M. and Corral, R. (2021), 'Numerical validation of an analytical seal flutter model', *Journal of the Global Power and Propulsion Society* **5**, 191–201.

Heners, J. P., Carraro, T., Frey, C. and Grüber, B. (2022), 'Evaluating the aerodynamic damping at shock wave boundary layer interacting flow conditions with harmonic balance', *Proceedings of ASME Turbo Expo 2022* . GT2022-81689.

Kato, M. and Launder, B. E. (1993), The modeling of turbulent flow around stationary and vibrating square cylinders, *in* '9th Symposium on Turbulent Shear Flows', pp. 10.4.1–10.4.6.

Kersken, H.-P., Ashcroft, G. and Frey, C. (2016), A hybrid mesh harmonic balance solver for the aeroelastic analysis of turbomachinery, *in* V. P. M. Papadrakakis, G. Stefanou and V. Plevris, eds, 'VII European Congress on Computational Methods in Applied Sciences and Engineering'.
URL: *https://eccomas2016.org/proceedings/pdf/7406.pdf*

Kersken, H.-P., Ashcroft, G., Frey, C., Wolfrum, N. and Korte, D. (2014), Nonreflecting boundary conditions for aeroelastic analysis in time and frequency domain 3D RANS solvers, *in* 'Proceedings of ASME Turbo Expo 2014'.

Müller, M., Kersken, H.-P. and Frey, C. (2022), A log-w turbulence model formulation for flutter analysis with harmonic balance, *in* '16th International Symposium on Unsteady Aerodynamics, Aeroacoustics & Aeroelasticity of Turbomachines (ISUAAAT16)'.
URL: *https://elib.dlr.de/188533/*

Sivel, P., Kersken, H.-P., Frey, C. and Kügeler, E. (2024), 'A low mach preconditioned harmonic balance solver for cavity flutter computations', *To be published in Proceedings of ASME Turbo Expo 2024* . GT2024-127337.

Thomas, J. L., Diskin, B. and Nishikaw, H. (2011), 'A critical study of agglomerated multigrid methods for diffusion on highly-stretched grids', *Comput. Fluids* **41**, 82–93.

Wilcox, D. C. (2006), *Turbulence Modeling for CFD*, 3 edn, DCW Industries, La Cañada, USA.